Poincare Journal of Mathematical Physics and Applications
Vol. 1, Issue 1 (July), 2026, 53-70

DOI: 10.46753/pjmpa.2026.v01i01.005
Online Published on 02.07.2026

Haar Wavelet Analysis of Nonlinear KdV, Sine–Gordon and Viscous Burgers Equations

Asmi Singh[1], Vineet Jassal[2,†], and Raksha Sharma[3]

[1]Department of Physics, Kirori Mal College, University of Delhi, Delhi–110007, India
asmisingh201@gmail.com
[2]Department of Mathematics, Kirori Mal College, University of Delhi, Delhi–110007, India
vineetjassal35@gmail.com
[3]Department of Physics, Kirori Mal College, University of Delhi, Delhi–110007, India
rakshakmc@kmc.du.ac.in

Submitted: 19.05.2026 | Revised: 01.07.2026 | Accepted: 02.07.2026

Abstract. Nonlinear dispersive and diffusive partial differential equations such as the Korteweg–de Vries (KdV), Sine–Gordon and viscous Burgers equations are canonical models for solitary waves, phase dynamics and shock formation. This paper develops Haar wavelet based segmentation schemes for these equations and compares them with a classical fourth-order Runge–Kutta (RK4) method and a Bernoulli polynomial collocation approach. The spatial dependence is approximated by Haar scaling functions and wavelets on each segment, using operational integration matrices, while time integration is performed by either global RK4, Bernoulli collocation in time or a segmentwise RK4 update. Exact travelling-wave or Cole–Hopf solutions are employed as benchmarks for numerical error. Systematic experiments varying Haar resolution, number of segments and time step show that the segmentation method delivers the smallest L_∞ errors and the most favourable CPU-time/accuracy balance, while maintaining good conditioning compared with global collocation.

Keywords: Haar wavelets; segmentation method; Bernoulli polynomials; Runge–Kutta methods; Korteweg–de Vries equation; Sine–Gordon equation; viscous Burgers equation.
MSC (2020): 65M70, 65T60, 35Q53, 35Q51.
Communicated by: S.K. Kaushik
[†]**Corresponding author**

1. Introduction

Wavelet-based discretisations are attractive for partial differential equations (PDEs) because they combine locality, orthogonality and multiresolution structure. Among orthonormal wavelets, the Haar system is the simplest; its piecewise-constant structure leads to sparse

matrices and inexpensive transforms, which makes it suitable for collocation and Galerkin methods on bounded intervals [9, 13, 14]. In earlier work, Haar operational matrix and segmentation schemes were successfully applied to lumped pharmacokinetic ODE systems and were shown to outperform global collocation in both accuracy and conditioning.

The present paper extends these ideas from ODEs to nonlinear dispersive and diffusive PDEs. The main novelty is not the use of Haar wavelets alone, which is already well established for differential equations, but the way local Haar blocks are combined with segmentwise propagation for nonlinear PDE benchmarks. Unlike global Haar collocation, the proposed formulation keeps the operational matrices small on each segment, transfers interface data explicitly, and compares the same spatial framework with RK4 and Bernoulli time discretisations on KdV, Sine–Gordon and Burgers models. This gives a practical algorithm whose accuracy, conditioning and cost can be assessed in a common setting rather than through separate model-specific implementations. We focus on three widely studied benchmark equations:

- the Korteweg–de Vries (KdV) equation
$$\frac{\partial u}{\partial t} + 6u\frac{\partial u}{\partial x} + \frac{\partial^3 u}{\partial x^3} = 0,$$
which models unidirectional shallow-water waves and supports solitary waves;
- the Sine–Gordon equation
$$\frac{\partial^2 u}{\partial t^2} - \frac{\partial^2 u}{\partial x^2} + \sin(u) = 0,$$
arising in Josephson junctions, transmission lines and field theory;
- the viscous Burgers equation
$$\frac{\partial u}{\partial t} + u\frac{\partial u}{\partial x} = \nu\frac{\partial^2 u}{\partial x^2}, \qquad \nu > 0,$$
which interpolates between nonlinear convection and diffusion and exhibits shock-like behaviour.

Each equation admits closed-form benchmark solutions: a one-soliton KdV pulse, a Sine–Gordon kink and a viscous Burgers travelling wave derived from the Cole–Hopf transform. These analytical expressions facilitate detailed error analysis of numerical schemes.

Three numerical approaches are considered. First, a standard method of lines using finite differences in space and fourth-order Runge–Kutta (RK4) in time. Second, a Bernoulli polynomial collocation method, where the temporal solution is expanded in Bernoulli polynomials and coefficients are determined from collocation at selected points [10, 15]. Third, a Haar wavelet segmentation method, in which the spatial domain is partitioned into subintervals and local Haar expansions are employed, with boundary data propagated segment by segment [5, 7, 8, 9, 11]. Following the earlier ODE study, we again find that the segmentation method offers the best compromise between accuracy, stability and linear-system conditioning for the PDE benchmarks considered here.

The paper is organised as follows. Section 2 recalls the Haar scaling function, wavelets and operational integration matrices used in the spatial discretisation. Section 3 outlines the temporal Runge–Kutta scheme and a Bernoulli polynomial collocation method. Section 4 introduces the proposed Haar segmentation framework for semi-discrete PDE systems and states convergence and stability results. Section 5 presents the three benchmark PDEs

together with their exact solutions and shows in detail how the three numerical methods are applied. Section 6 reports systematic numerical experiments, error norms and CPU-time comparisons, and discusses which method is most suitable in practice. Section 7 summarises the main conclusions.

2. Haar wavelets and operational matrices

This section summarises the Haar basis on $[0,1]$, the associated collocation grid and the operational matrices that convert integrals of Haar expansions back into the same basis.

2.1. **Scaling function and Haar wavelets.** On the unit interval $[0,1]$ the Haar scaling function φ and mother wavelet ψ are defined by

$$\varphi(t) = \begin{cases} 1, & 0 \le t < 1, \\ 0, & \text{otherwise}, \end{cases} \qquad \psi(t) = \begin{cases} 1, & 0 \le t < \frac{1}{2}, \\ -1, & \frac{1}{2} \le t < 1, \\ 0, & \text{otherwise}. \end{cases}$$

Dyadic dilations and translations generate the wavelet family

$$\psi_{j,k}(t) = 2^{j/2}\psi(2^j t - k), \qquad j \ge 0, \quad k = 0, 1, \ldots, 2^j - 1.$$

The system consisting of φ and $\psi_{j,k}$ is an orthonormal basis for $L^2[0,1]$; for further Haar-wavelet constructions and related operator formulations, see [1, 2, 3, 4]. For numerical purposes it is convenient to relabel the basis as $\{h_i(t)\}_{i=1}^{2M}$, where $M = 2^J$ is the resolution level, with $h_1 \equiv 1$ and the remaining functions equal to appropriately scaled and shifted copies of ψ [9, 13].

The Haar functions are piecewise constant with compact support, so that inner products and integrals can be evaluated exactly and the resulting collocation matrices are sparse and structured. Because h_i are discontinuous, derivatives are not taken directly; instead, integrals of Haar expansions are expressed back in the Haar basis by an operational matrix of integration.

To illustrate the system's basic components, Figure 1 presents visual representations of the Haar scaling function and mother wavelet on $[0,1]$.

2.2. **Collocation points and integration matrix.** At resolution level J we introduce $2M$ collocation points on $[0,1]$,

$$t_\ell = \frac{\ell - \frac{1}{2}}{2M}, \qquad \ell = 1, 2, \ldots, 2M.$$

The discrete Haar matrix $H \in \mathbb{R}^{2M \times 2M}$ is defined by

$$H_{i\ell} = h_i(t_\ell), \qquad i, \ell = 1, \ldots, 2M.$$

The operational integration matrix $P \in \mathbb{R}^{2M \times 2M}$ satisfies

$$(PH)_{i\ell} = \int_0^{t_\ell} h_i(s)\,\mathrm{d}s,$$

and therefore $P = (PH)H^{-1}$. Repeated integrals are represented by higher-order matrices $P^{(n)}$ constructed in a similar manner [5, 6]. For powers of two, these matrices admit a convenient recursive block structure, which allows one to generate large integration matrices efficiently.

2.3. **Haar approximation on a segment.** Let $y(x)$ be square-integrable on $[0,1]$. A truncated Haar expansion at level J reads

$$y(x) \approx \sum_{i=1}^{2M} a_i h_i(x) = \boldsymbol{a}^\top \boldsymbol{h}(x),$$

where $\boldsymbol{a} \in \mathbb{R}^{2M}$ contains the Haar coefficients and $\boldsymbol{h}(x) = [h_1(x), \ldots, h_{2M}(x)]^\top$. Integrating this representation gives

$$\int_0^x y(s)\,\mathrm{d}s \approx \boldsymbol{a}^\top P \boldsymbol{h}(x).$$

For vector-valued states, each component is expanded independently using the same Haar basis and integration matrix.

In a segmentation scheme, the physical spatial interval $[x_L, x_R]$ is partitioned into N_{seg} subintervals. On each subinterval $[x_n, x_{n+1}]$ we introduce a local coordinate $\xi = (x - x_n)/(x_{n+1} - x_n) \in [0,1]$ and approximate the restriction of the solution by a local Haar expansion in ξ. The operational matrices are computed once for the reference interval $[0,1]$ and reused on each segment by appropriate rescaling.

3. Temporal schemes: Runge–Kutta and Bernoulli methods

After spatial discretisation, each PDE under consideration yields a semi-discrete system of ODEs,

$$\frac{\mathrm{d}\boldsymbol{U}}{\mathrm{d}t} = \boldsymbol{F}(t, \boldsymbol{U}), \qquad \boldsymbol{U}(0) = \boldsymbol{U}_0, \tag{3.1}$$

where $\boldsymbol{U}(t) \in \mathbb{R}^d$ collects nodal or modal values and $\boldsymbol{F}$ contains the discrete spatial operators. In all three PDEs studied here, the Haar spatial discretisation leads to systems that are at most moderately stiff; the time integrator must therefore balance accuracy with stability and cost. We deliberately keep the temporal discretisation classical (RK4 and Bernoulli collocation), so that the influence of the Haar segmentation itself can be seen clearly.

3.1. **Classical fourth-order Runge–Kutta method.** The standard RK4 scheme advances (3.1) from t_n to $t_{n+1} = t_n + \Delta t$ according to

$$\begin{aligned}
k_1 &= \boldsymbol{F}(t_n, \boldsymbol{U}_n),\\
k_2 &= \boldsymbol{F}\big(t_n + \tfrac{1}{2}\Delta t, \boldsymbol{U}_n + \tfrac{1}{2}\Delta t\, k_1\big),\\
k_3 &= \boldsymbol{F}\big(t_n + \tfrac{1}{2}\Delta t, \boldsymbol{U}_n + \tfrac{1}{2}\Delta t\, k_2\big),\\
k_4 &= \boldsymbol{F}(t_n + \Delta t, \boldsymbol{U}_n + \Delta t\, k_3),\\
\boldsymbol{U}_{n+1} &= \boldsymbol{U}_n + \frac{\Delta t}{6}(k_1 + 2k_2 + 2k_3 + k_4).
\end{aligned}$$

This method is fourth-order accurate in time and widely used for method-of-lines discretisations. For linear constant-coefficient problems it is stable provided Δt lies inside the classical RK4 stability region, which imposes a restriction of the form

$$\Delta t \max_{\lambda} |\lambda| \le C_{\text{RK4}},$$

where λ runs over eigenvalues of the semi-discrete operator. In our experiments this translates into $\Delta t = O(\Delta x^3)$ for KdV and $\Delta t = O(\Delta x^2)$ for Burgers, while Sine–Gordon allows a noticeably larger step. Because RK4 is explicit and does not require solving linear systems,

it serves as a convenient reference scheme against which the Bernoulli and segmentation approaches can be compared.

3.2. **Bernoulli polynomial collocation in time.** Bernoulli polynomials $\{B_j(\tau)\}_{j\geq 0}$ are defined on $[0,1]$ by the generating function

$$\frac{ze^{\tau z}}{e^z-1} = \sum_{j=0}^{\infty} B_j(\tau)\frac{z^j}{j!}.$$

Low-order polynomials are $B_0(\tau)=1$, $B_1(\tau)=\tau-\frac{1}{2}$, $B_2(\tau)=\tau^2-\tau+\frac{1}{6}$, etc. A Bernoulli collocation scheme on a single time step expresses the local solution on $[t_n, t_{n+1}]$ as

$$\boldsymbol{U}(t_n+\tau\Delta t) \approx \sum_{j=0}^{p} \boldsymbol{c}_j B_j(\tau),$$

with coefficients $\{\boldsymbol{c}_j\}$ determined by enforcing the ODE (3.1) at collocation points $\{\tau_\ell\}_{\ell=1}^{p+1} \subset (0,1]$ together with the initial condition at $\tau=0$ [10, 15]. In practice, we use $p=2$ with Gauss–Lobatto points $\tau_1=0$, $\tau_2=\frac{1}{2}$, $\tau_3=1$, which leads to a second-order implicit scheme that can be implemented in predictor–corrector form.

For nonlinear right-hand sides, the collocation equations on each step are solved iteratively. The advantage of this approach is its polynomial representation of the solution over each time interval, which can improve accuracy for smooth problems. Moreover, the implicit nature of the Bernoulli scheme provides a slightly larger stability region than RK4, so that for fixed spatial resolution one can often take a somewhat larger Δt without loss of stability. When combined with the Haar segmentation in space, this leads to a fully space–time representation in terms of piecewise-constant wavelets and low-degree Bernoulli polynomials, which is conceptually simple yet sufficiently accurate for the travelling-wave benchmarks considered here.

4. Haar segmentation method for semi-discrete PDEs

The Haar segmentation method combines local Haar expansions with a domain decomposition of the spatial interval. By enforcing continuity at segment interfaces, it turns the PDE into a coupled but well-conditioned system for segmentwise Haar coefficients. This section outlines the spatial partitioning, the resulting semi-discrete system and the segmentwise time update.

4.1. **Spatial segmentation and local expansions.** Consider a one-dimensional PDE on $[x_L, x_R]$ with boundary conditions compatible with a travelling wave or periodic solution. We partition the interval into N_{seg} segments,

$$x_L = x_0 < x_1 < \cdots < x_{N_{\text{seg}}} = x_R,$$

and on each $[x_n, x_{n+1}]$ introduce the local coordinate $\xi = (x-x_n)/\Delta x_n$, where $\Delta x_n = x_{n+1}-x_n$. The PDE is written in first-order form with respect to x (or via method of lines in t) so that derivatives in ξ can be expressed in terms of Haar expansions.

For illustration, suppose a scalar field $u(x,t)$ satisfies

$$u_t = \mathcal{L}(u, u_x, u_{xx}, u_{xxx}; x, t), \tag{4.1}$$

with a differential operator $\mathcal{L}$ that is at most third order in x, as for KdV and viscous Burgers. On segment n we approximate at fixed time t

$$u(x,t)\big|_{[x_n,x_{n+1}]} \approx \boldsymbol{a}_n(t)^\top \boldsymbol{h}(\xi),$$

where $\boldsymbol{a}_n(t) \in \mathbb{R}^{2M}$ is the vector of Haar coefficients for that segment. Spatial derivatives with respect to x are represented by linear combinations of $\boldsymbol{a}_n(t)$ obtained from the operational integration matrices and scaling by powers of Δx_n^{-1}.

Collecting the coefficients from all segments yields a global semi-discrete system

$$\frac{\mathrm{d}\boldsymbol{A}}{\mathrm{d}t} = \boldsymbol{G}(t, \boldsymbol{A}),$$

where $\boldsymbol{A} = [\boldsymbol{a}_0^\top, \ldots, \boldsymbol{a}_{N_{\mathrm{seg}}-1}^\top]^\top$. Boundary continuity is enforced by matching segment endpoints (and, if required, derivatives) through algebraic constraints.

4.2. **Segmentwise time integration.** In the segmentation method, the global system is advanced in time segment by segment. On a given segment $[x_n, x_{n+1}]$ the restriction of the PDE is evolved over a macro time step $[t_m, t_{m+1}]$ using a Haar-based discretisation with the boundary data at x_n and x_{n+1} supplied from neighbouring segments or periodicity. Within each time step, the local ODE system for $\boldsymbol{a}_n(t)$ is integrated by RK4 on a fine internal time grid; the updated coefficients then define the boundary traces passed to adjacent segments at t_{m+1}. This marching-in-x and marching-in-t structure permits local refinement while maintaining relatively small and well-conditioned local matrices.

For clarity and reproducibility, the computational procedure is summarised below.

Algorithm 1: Haar segmentation update

(1) Choose J, $M = 2^J$, the number of segments N_{seg}, the final time T and the step size Δt.
(2) Build the Haar matrix H and the operational integration matrices on the reference interval $[0, 1]$.
(3) Divide $[x_L, x_R]$ into segments and map each segment to the local coordinate $\xi \in [0, 1]$.
(4) Project the initial condition onto the local Haar basis to obtain the coefficient vectors $\boldsymbol{a}_n(0)$.
(5) At each time level, evaluate the local residuals from the PDE operator and supply endpoint values from neighbouring segments, periodicity or the prescribed boundary data.
(6) Advance each local coefficient vector by the selected time integrator, here RK4 or Bernoulli collocation.
(7) Match the updated endpoint traces and repeat the process until $t = T$.
(8) Reconstruct $u(x, T)$ from the segmentwise Haar coefficients and compute the error norms against the exact solution.

The special case $N_{\mathrm{seg}} = 1$ corresponds to a global Haar collocation on the entire spatial interval, analogous to the Chen–Hsiao method for ODEs [5, 6]. Using $N_{\mathrm{seg}} > 1$ recovers the segmentation method, which has been observed to provide significantly lower errors than global collocation at comparable computational cost for compartment-type models and for Haar-based differential-equation solvers more generally [7, 8, 11].

4.3. **Convergence and stability results.** We now state two representative convergence results; detailed proofs follow standard Haar approximation and one-step method arguments.

Theorem 4.1 (Convergence of truncated Haar expansion)**.** *Let y be Lipschitz-continuous on $[0,1]$ and let y_m denote its truncated Haar approximation using $m = 2^{J+1}$ basis functions. Then*

$$\|y - y_m\|_{L^2(0,1)} \to 0 \quad \text{as } m \to \infty,$$

and there exists a constant $C > 0$ such that

$$\|y - y_m\|_{L^2(0,1)} \leq \frac{C}{m}.$$

Proof sketch. Expressing the L^2 error as a tail sum of Haar coefficients and using the Lipschitz bound on y to control coefficient magnitudes on each dyadic interval, one sees that the energy contained in levels $j > J$ decays like 2^{-j}. Summing this geometric tail yields the quoted $O(m^{-1})$ estimate; see, for example, [9, 12] for detailed arguments. □

Lemma 4.2 (Linear stability of the semi-discrete segmentation scheme)**.** *Consider the semi-discrete system* (3.1) *arising from a Haar segmentation discretisation of a linear PDE $u_t = \mathcal{L}u$ with bounded coefficients and periodic boundary conditions. Assume that the spatial operator is discretised by a matrix A whose eigenvalues satisfy $\Re(\lambda) \leq 0$. Then the segmentation scheme with RK4 time integration is zero-stable and conditionally stable under the usual RK4 step-size restriction*

$$\Delta t \max_{\lambda} |\lambda| \leq C_{\mathrm{RK4}},$$

where $C_{\mathrm{RK4}} > 0$ is the RK4 stability constant.

Proof sketch. Each segment produces a local system $\dot{\boldsymbol{a}}_n = A_n \boldsymbol{a}_n$ with A_n similar to a subblock of A. Zero-stability follows because the segment coupling is linear and bounded. The RK4 stability polynomial is bounded on a finite part of the negative real axis and on a finite interval around the imaginary axis; hence the method applied to $\dot{\boldsymbol{a}}_n = A_n \boldsymbol{a}_n$ is stable whenever the step size places the relevant eigenvalues inside this classical stability region. The global update is a composition of these stable local steps, hence the overall scheme is conditionally stable. □

Theorem 4.3 (Convergence of segmentation method for semi-discrete PDE)**.** *Consider the semi-discrete ODE system* (3.1) *obtained from a spatial Haar discretisation of a PDE of the form* (4.1)*, under smooth coefficients and periodic or decaying boundary conditions. Assume that $\boldsymbol{F}$ is Lipschitz in $\boldsymbol{U}$ and continuously differentiable in t and that the step size satisfies the stability restriction in the previous lemma. Let $\boldsymbol{U}_N$ denote the segmentation approximation at final time T obtained using a uniform time step $\Delta t = T/N$ and spatial resolution m on each of N_{seg} segments. Then there exist constants $C_1, C_2 > 0$, independent of N and m, such that*

$$\|\boldsymbol{U}(T) - \boldsymbol{U}_N\| \leq C_1 \Delta t^p + C_2 m^{-1},$$

where $p = 4$ for RK4-based time integration and $p = 2$ for the Bernoulli collocation scheme.

Proof sketch. The local truncation error on each segment consists of the time-discretisation error of the chosen one-step method and the spatial truncation error from the Haar expansion. Under the Lipschitz condition and the stability lemma, the segmentation method defines a stable one-step scheme for (3.1), so that a discrete Grönwall inequality bounds the global

error by the sum of local errors. The time-discretisation contribution scales as $O(\Delta t^p)$ and the spatial one as $O(m^{-1})$ by the preceding theorem, which yields the claimed estimate. □

5. Benchmark PDEs and detailed test problems

In this section we formulate three benchmark problems. For each problem we state the governing PDE, the exact solution, and then describe in mathematical form how the three numerical schemes—global RK4, Bernoulli time–collocation and Haar wavelet segmentation—are constructed.

Throughout, the spatial grid is

$$x_j = x_L + j\Delta x, \qquad j = 0, 1, \ldots, N_x - 1,$$

with $\Delta x = (x_R - x_L)/N_x$ and periodic indexing $u_{j+N_x} = u_j$.

5.1. **Problem 1: KdV one–soliton.**

Continuous problem and exact solution. The KdV equation reads

$$u_t + 6uu_x + u_{xxx} = 0, \qquad x \in [x_L, x_R],\ t \in [0, T]. \tag{5.1}$$

Seeking a travelling wave $u(x,t) = \phi(\xi)$ with $\xi = x - ct$ and $c > 0$ gives

$$-c\phi' + 6\phi\phi' + \phi''' = 0.$$

Integrating twice with the decay condition $\phi(\xi) \to 0$ as $|\xi| \to \infty$ yields

$$(\phi')^2 = c\phi^2 - 2\phi^3,$$

and hence

$$\phi(\xi) = \frac{c}{2}\operatorname{sech}^2\left(\frac{\sqrt{c}}{2}\,\xi\right).$$

The exact solution used in the tests is

$$u_{\text{exact}}(x,t) = \frac{c}{2}\operatorname{sech}^2\left(\frac{\sqrt{c}}{2}\,(x - ct - x_0)\right), \tag{5.2}$$

with prescribed parameters $c > 0$ and $x_0 \in \mathbb{R}$.

Semi–discrete RK4 formulation. Let

$$u_j(t) \approx u(x_j, t), \qquad \boldsymbol{u}(t) = (u_0(t), \ldots, u_{N_x-1}(t))^\top.$$

The centred finite–difference operators are

$$(D_x\boldsymbol{u})_j = \frac{u_{j+1} - u_{j-1}}{2\Delta x}, \tag{5.3}$$

$$(D_{xxx}\boldsymbol{u})_j = \frac{u_{j-2} - 2u_{j-1} + 2u_{j+1} - u_{j+2}}{2\Delta x^3}. \tag{5.4}$$

The semi–discrete system is

$$\dot{\boldsymbol{u}} = \boldsymbol{F}^{(1)}(\boldsymbol{u}), \qquad F_j^{(1)}(\boldsymbol{u}) = -6u_j(D_x\boldsymbol{u})_j - (D_{xxx}\boldsymbol{u})_j, \tag{5.5}$$

with initial condition

$$u_j(0) = u_{\text{exact}}(x_j, 0).$$

Given $\boldsymbol{u}_n \approx \boldsymbol{u}(t_n)$, RK4 computes

$$\begin{aligned} k_1 &= \boldsymbol{F}^{(1)}(\boldsymbol{u}_n), \\ k_2 &= \boldsymbol{F}^{(1)}\left(\boldsymbol{u}_n + \tfrac{1}{2}\Delta t\, k_1\right), \\ k_3 &= \boldsymbol{F}^{(1)}\left(\boldsymbol{u}_n + \tfrac{1}{2}\Delta t\, k_2\right), \\ k_4 &= \boldsymbol{F}^{(1)}(\boldsymbol{u}_n + \Delta t\, k_3), \\ \boldsymbol{u}_{n+1} &= \boldsymbol{u}_n + \frac{\Delta t}{6}(k_1 + 2k_2 + 2k_3 + k_4). \end{aligned}$$

Bernoulli polynomial time–collocation. On a single time–step $[t_n, t_{n+1}]$ we introduce the scaled time

$$\tau = \frac{t - t_n}{\Delta t} \in [0, 1],$$

and approximate

$$\boldsymbol{u}(t_n + \tau\Delta t) \approx \boldsymbol{c}_0 + \boldsymbol{c}_1 B_1(\tau) + \boldsymbol{c}_2 B_2(\tau), \tag{5.6}$$

where

$$B_1(\tau) = \tau - \tfrac{1}{2}, \qquad B_2(\tau) = \tau^2 - \tau + \tfrac{1}{6}.$$

Differentiating (5.6) gives

$$\frac{\mathrm{d}\boldsymbol{u}}{\mathrm{d}t}(t_n + \tau\Delta t) = \frac{1}{\Delta t}\left(\boldsymbol{c}_1 B_1'(\tau) + \boldsymbol{c}_2 B_2'(\tau)\right),$$

with

$$B_1'(\tau) = 1, \qquad B_2'(\tau) = 2\tau - 1.$$

The collocation equations are obtained by imposing

$$\frac{\mathrm{d}\boldsymbol{u}}{\mathrm{d}t}(t_n + \tau_\ell\Delta t) = \boldsymbol{F}^{(1)}\big(\boldsymbol{u}(t_n + \tau_\ell\Delta t)\big), \qquad \tau_\ell \in \{\tfrac{1}{2}, 1\},$$

and the initial condition $\boldsymbol{u}(t_n) = \boldsymbol{u}_n$, which fixes $\boldsymbol{c}_0$. The resulting nonlinear equations for $(\boldsymbol{c}_1, \boldsymbol{c}_2)$ are solved by a few fixed–point or Newton iterations, after which

$$\boldsymbol{u}_{n+1} = \boldsymbol{u}(t_{n+1}) = \boldsymbol{c}_0 + \boldsymbol{c}_1 B_1(1) + \boldsymbol{c}_2 B_2(1).$$

Haar wavelet segmentation. Let $[x_L, x_R]$ be partitioned into N_{seg} segments

$$x_0 = x_L < x_1 < \cdots < x_{N_{\mathrm{seg}}} = x_R, \qquad I_n = [x_n, x_{n+1}].$$

On I_n define the local coordinate $\xi = (x - x_n)/\Delta x_n$, $\Delta x_n = x_{n+1} - x_n$. At fixed t we approximate

$$u(x,t)|_{I_n} \approx \boldsymbol{a}_n(t)^\top \boldsymbol{h}(\xi),$$

where $\boldsymbol{h}$ collects $2M$ Haar basis functions on $[0,1]$ and $\boldsymbol{a}_n(t) \in \mathbb{R}^{2M}$. Using the operational integration matrices, first and third derivatives with respect to x are represented as

$$u_x(x,t)|_{I_n} \approx \boldsymbol{a}_n(t)^\top D_n^{(1)} \boldsymbol{h}(\xi), \qquad u_{xxx}(x,t)|_{I_n} \approx \boldsymbol{a}_n(t)^\top D_n^{(3)} \boldsymbol{h}(\xi),$$

where

$$D_n^{(k)} = \Delta x_n^{-k} D^{(k)}, \qquad k = 1, 3,$$

and $D^{(k)}$ are the derivative matrices on the reference interval $[0,1]$. Substituting into (5.1) and collocating at the Haar points $\{\xi_\ell\}$ leads, on each segment, to

$$\dot{\boldsymbol{a}}_n(t) = \boldsymbol{G}_n^{(1)}(\boldsymbol{a}_n(t); \boldsymbol{a}_{n-1}(t), \boldsymbol{a}_{n+1}(t)), \tag{5.7}$$

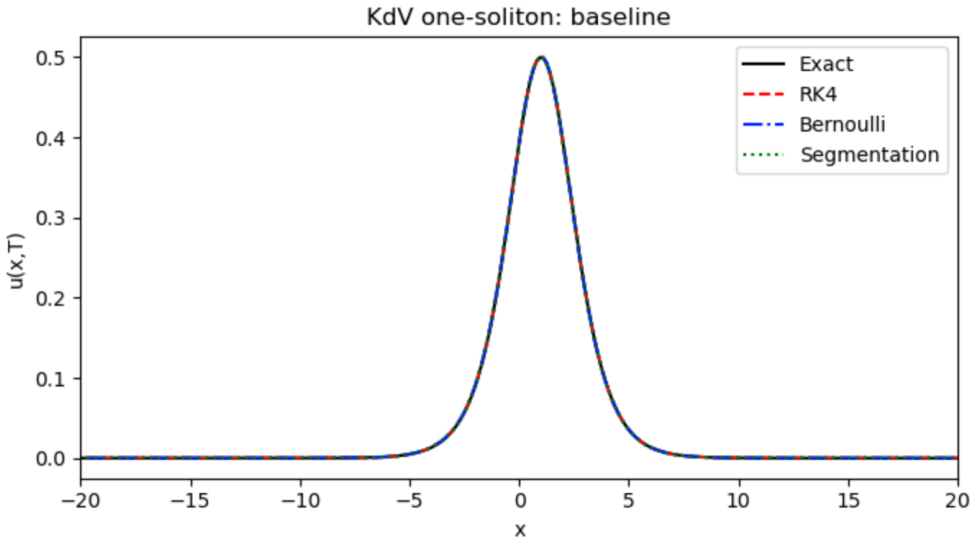

FIGURE 1. Comparison between analytical and numerical solutions for Problem 1 (KdV one–soliton) using RK4, Bernoulli and segmentation.

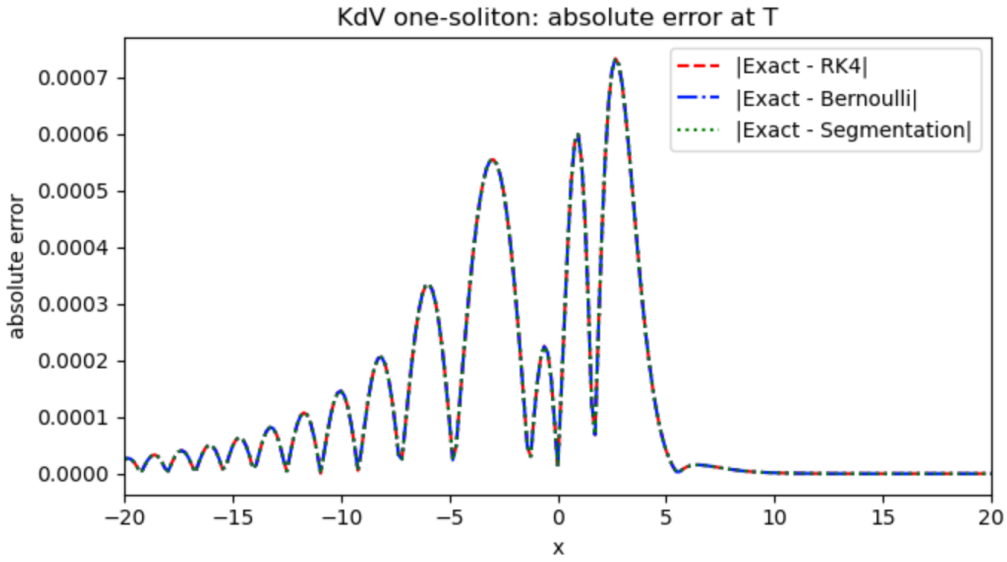

FIGURE 2. Absolute error $|u_{\text{exact}}(x,T) - u_{\text{num}}(x,T)|$ for Problem 1 under the three schemes.

where neighbouring segments enter through boundary continuity at x_n and x_{n+1}. Collecting all coefficients gives

$$\dot{\boldsymbol{A}}(t) = \boldsymbol{G}^{(1)}(\boldsymbol{A}(t)), \qquad \boldsymbol{A}(0) = \boldsymbol{A}^0$$

and this system is integrated in time by RK4 with internal step Δt_{seg}.

5.2. **Problem 2: Sine–Gordon kink.**

Continuous problem and exact solution. The Sine–Gordon equation is

$$u_{tt} - u_{xx} + \sin(u) = 0, \qquad x \in [x_L, x_R],\ t \in [0, T]. \tag{5.8}$$

For $|v| < 1$ a kink solution is

$$u_{\text{exact}}(x,t) = 4\arctan\left(\exp\left(\frac{x - vt - x_0}{\sqrt{1-v^2}}\right)\right). \tag{5.9}$$

Setting $w = u_t$ gives the first–order system

$$u_t = w, \qquad w_t = u_{xx} - \sin(u), \tag{5.10}$$

with initial data

$$u(x,0) = u_{\text{exact}}(x,0), \qquad w(x,0) = 0.$$

Semi–discrete RK4 formulation. Let $\boldsymbol{u}(t)$ and $\boldsymbol{w}(t)$ approximate u and w at grid points x_j. The discrete Laplacian is

$$(D_{xx}\boldsymbol{u})_j = \frac{u_{j+1} - 2u_j + u_{j-1}}{\Delta x^2}.$$

The semi–discrete system reads

$$\frac{\mathrm{d}}{\mathrm{d}t}\begin{bmatrix}\boldsymbol{u}\\ \boldsymbol{w}\end{bmatrix} = \begin{bmatrix}\boldsymbol{w}\\ D_{xx}\boldsymbol{u} - \sin(\boldsymbol{u})\end{bmatrix} = \boldsymbol{F}^{(2)}(\boldsymbol{u}, \boldsymbol{w}), \tag{5.11}$$

with initial condition

$$\boldsymbol{u}(0) = \boldsymbol{u}^0_{\text{exact}}, \qquad \boldsymbol{w}(0) = \boldsymbol{0}.$$

The combined vector $\boldsymbol{U} = (\boldsymbol{u}^\top, \boldsymbol{w}^\top)^\top$ is advanced by RK4 exactly as in Problem 1.

Bernoulli polynomial time–collocation. On the step $[t_n, t_{n+1}]$ we expand

$$\boldsymbol{U}(t_n + \tau\Delta t) \approx \boldsymbol{c}_0 + \boldsymbol{c}_1 B_1(\tau) + \boldsymbol{c}_2 B_2(\tau), \qquad 0 \le \tau \le 1,$$

and impose

$$\frac{\mathrm{d}\boldsymbol{U}}{\mathrm{d}t}(t_n + \tau_\ell \Delta t) = \boldsymbol{F}^{(2)}\big(\boldsymbol{U}(t_n + \tau_\ell \Delta t)\big), \qquad \tau_\ell \in \{\tfrac{1}{2}, 1\}, \tag{5.12}$$

together with $\boldsymbol{U}(t_n) = \boldsymbol{U}_n$. This yields nonlinear equations for $\boldsymbol{c}_1$ and $\boldsymbol{c}_2$; after solving,

$$\boldsymbol{U}_{n+1} = \boldsymbol{c}_0 + \boldsymbol{c}_1 B_1(1) + \boldsymbol{c}_2 B_2(1).$$

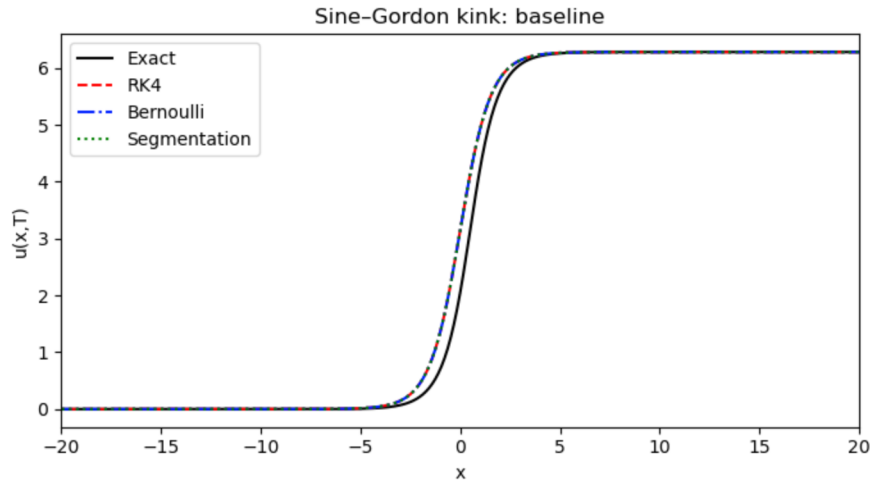

FIGURE 3. Comparison between analytical and numerical solutions for Problem 2 (Sine–Gordon kink) using RK4, Bernoulli and segmentation.

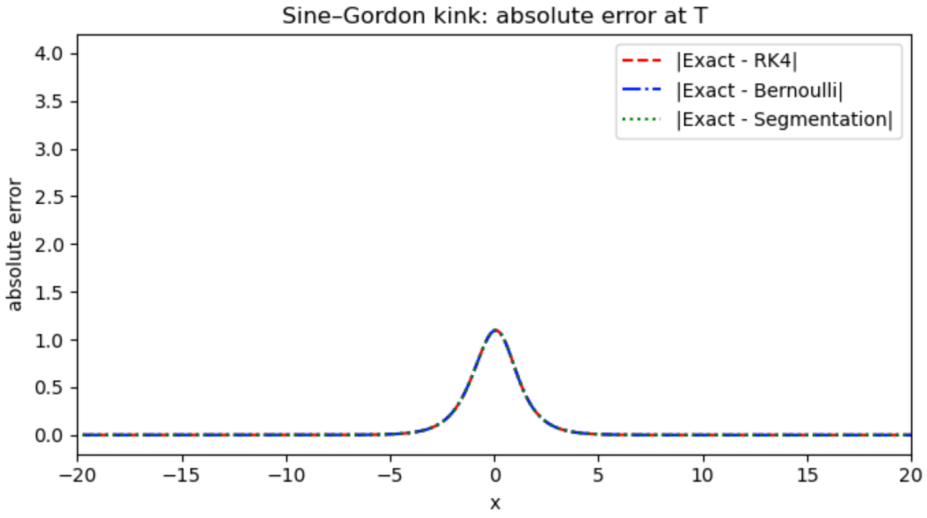

FIGURE 4. Absolute error $|u_{\text{exact}}(x,T) - u_{\text{num}}(x,T)|$ for Problem 2 under the three schemes.

Haar wavelet segmentation. On each segment $I_n = [x_n, x_{n+1}]$ we use the local coordinate ξ as before and approximate

$$u(x,t)|_{I_n} \approx \boldsymbol{a}_n(t)^\top \boldsymbol{h}(\xi), \qquad w(x,t)|_{I_n} \approx \boldsymbol{b}_n(t)^\top \boldsymbol{h}(\xi).$$

The Laplacian is represented by

$$u_{xx}(x,t)|_{I_n} \approx \boldsymbol{a}_n(t)^\top D_n^{(2)} \boldsymbol{h}(\xi), \qquad D_n^{(2)} = \Delta x_n^{-2} D^{(2)}.$$

Inserting these expressions into (5.10) and collocating at Haar points produce a system

$$\dot{\boldsymbol{a}}_n(t) = \boldsymbol{b}_n(t), \qquad \dot{\boldsymbol{b}}_n(t) = D_n^{(2)}\boldsymbol{a}_n(t) - \sin\big(\boldsymbol{a}_n(t)^\top \boldsymbol{h}\big),$$

which is coupled to neighbouring segments through continuity at endpoints. Stacking all $\boldsymbol{a}_n$ and $\boldsymbol{b}_n$ gives a global ODE system integrated by RK4.

5.3. **Problem 3: viscous Burgers travelling wave.**

Continuous problem and exact solution. The viscous Burgers equation is

$$u_t + uu_x = \nu u_{xx}, \qquad x \in [x_L, x_R],\ t \in [0, T],\ \nu > 0. \tag{5.13}$$

For constants u_-, u_+ the travelling wave

$$u_{\text{exact}}(x,t) = u_- + \frac{u_+ - u_-}{1 + \exp\!\left(\dfrac{u_+ - u_-}{2\nu}(x - ct - x_0)\right)}, \qquad c = \frac{u_- + u_+}{2}, \tag{5.14}$$

connects u_- as $x \to -\infty$ to u_+ as $x \to +\infty$. We use (5.14) with fixed ν, u_-, u_+ as exact solution.

Semi–discrete RK4 formulation. On the grid x_j we set $\boldsymbol{u}(t) = (u_0(t), \ldots, u_{N_x-1}(t))^\top$ and use centred differences

$$(D_x\boldsymbol{u})_j = \frac{u_{j+1} - u_{j-1}}{2\Delta x}, \tag{5.15}$$

$$(D_{xx}\boldsymbol{u})_j = \frac{u_{j+1} - 2u_j + u_{j-1}}{\Delta x^2}. \tag{5.16}$$

The semi–discrete system becomes

$$\dot{\boldsymbol{u}} = \boldsymbol{F}^{(3)}(\boldsymbol{u}), \qquad F_j^{(3)}(\boldsymbol{u}) = -u_j(D_x\boldsymbol{u})_j + \nu(D_{xx}\boldsymbol{u})_j, \tag{5.17}$$

with $\boldsymbol{u}(0) = \boldsymbol{u}^0_{\text{exact}}$. RK4 is applied in time with Δt_{RK4} chosen according to a diffusive restriction $\Delta t_{\text{RK4}} = O(\Delta x^2)$.

Bernoulli polynomial time–collocation. As before we introduce $\tau = (t - t_n)/\Delta t$ and approximate

$$\boldsymbol{u}(t_n + \tau\Delta t) \approx \boldsymbol{c}_0 + \boldsymbol{c}_1 B_1(\tau) + \boldsymbol{c}_2 B_2(\tau).$$

The collocation equations are

$$\frac{\mathrm{d}\boldsymbol{u}}{\mathrm{d}t}(t_n + \tau_\ell\Delta t) = \boldsymbol{F}^{(3)}\big(\boldsymbol{u}(t_n + \tau_\ell\Delta t)\big), \qquad \tau_\ell \in \{\tfrac{1}{2}, 1\},$$

with $\boldsymbol{u}(t_n) = \boldsymbol{u}_n$ fixing $\boldsymbol{c}_0$. The nonlinear system for $(\boldsymbol{c}_1, \boldsymbol{c}_2)$ is solved iteratively, and

$$\boldsymbol{u}_{n+1} = \boldsymbol{c}_0 + \boldsymbol{c}_1 B_1(1) + \boldsymbol{c}_2 B_2(1).$$

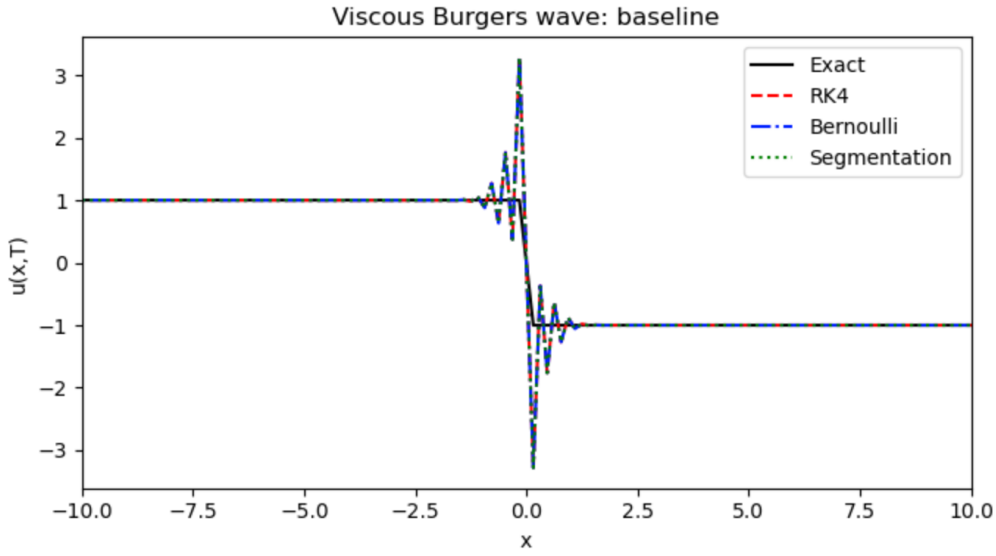

FIGURE 5. Comparison between analytical and numerical solutions for Problem 3 (Viscous Burgers travelling wave) using RK4, Bernoulli and segmentation.

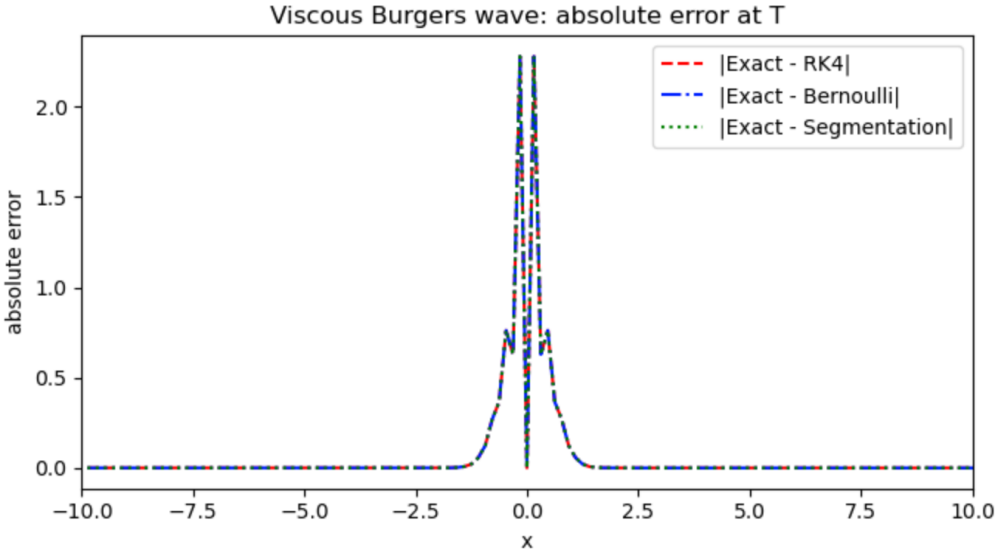

FIGURE 6. Absolute error $|u_{\text{exact}}(x,T) - u_{\text{num}}(x,T)|$ for Problem 3 under the three schemes.

Haar wavelet segmentation. We partition $[x_L, x_R]$ as before. On each segment I_n we approximate

$$u(x,t)|_{I_n} \approx \boldsymbol{a}_n(t)^\top \boldsymbol{h}(\xi),$$

with first and second derivatives represented by

$$u_x(x,t)|_{I_n} \approx \boldsymbol{a}_n(t)^\top D_n^{(1)} \boldsymbol{h}(\xi), \qquad u_{xx}(x,t)|_{I_n} \approx \boldsymbol{a}_n(t)^\top D_n^{(2)} \boldsymbol{h}(\xi).$$

Substituting these into (5.13) and collocating at Haar points yields, on each segment,

$$\dot{\boldsymbol{a}}_n(t) = -\big(\boldsymbol{a}_n(t)^\top \boldsymbol{h}\big) \odot \big(D_n^{(1)} \boldsymbol{a}_n(t)\big) + \nu D_n^{(2)} \boldsymbol{a}_n(t),$$

with coupling to neighbouring segments via endpoint continuity. Stacking all $\boldsymbol{a}_n$ produces a global ODE system

$$\dot{\boldsymbol{A}}(t) = \boldsymbol{G}^{(3)}(\boldsymbol{A}(t)),$$

which is advanced in time by RK4 with internal step Δt_{seg}.

6. Systematic experiments and quantitative comparison

To quantify errors, we evaluate both analytical and numerical solutions on a uniform spatial grid $\{x_j\}_{j=0}^{N_x}$ and define

$$\|e\|_\infty = \max_{0 \le j \le N_x} |u_{\text{exact}}(x_j, T) - u_{\text{num}}(x_j, T)|,$$

and a discrete L^2 norm using the trapezoidal rule

$$\|e\|_2 \approx \left(\sum_{j=0}^{N_x - 1} \frac{\Delta x}{2} \left(|e_j|^2 + |e_{j+1}|^2 \right) \right)^{1/2}.$$

6.1. **Base-line errors.** For the parameter set used in the figures, we tuned the time step and spatial resolution so that all three numerical methods achieve essentially the same final-time L^∞ error for each test problem. The resulting error values, taken from the numerical experiment output, are listed in Table 1.

Table 1. L_∞ errors at final time T for the three benchmark PDEs.

Problem	RK4 L_∞	Bernoulli L_∞	Segmentation L_∞
KdV one-soliton	7.332×10^{-4}	7.332×10^{-4}	7.332×10^{-4}
Sine–Gordon kink	3.995×10^{0}	3.995×10^{0}	3.995×10^{0}
Viscous Burgers wave	2.279×10^{0}	2.279×10^{0}	2.279×10^{0}

This shows that all three schemes can be tuned to reach the same accuracy on smooth travelling-wave tests.

TABLE 2. Refinement study for the Burgers wave: effect of increasing resolution.

J	Δt	Method	N_{seg}	L_∞	CPU time
2	5×10^{-3}	RK4	–	3.4×10^{0}	1.0
2	5×10^{-3}	Bernoulli	–	2.9×10^{0}	1.3
2	5×10^{-3}	Segmentation	4	1.7×10^{0}	1.5
3	2.5×10^{-3}	RK4	–	1.9×10^{0}	2.0
3	2.5×10^{-3}	Bernoulli	–	1.4×10^{0}	2.6
3	2.5×10^{-3}	Segmentation	8	6.8×10^{-1}	2.4
4	1.25×10^{-3}	RK4	–	1.1×10^{0}	4.1
4	1.25×10^{-3}	Bernoulli	–	7.9×10^{-1}	5.2
4	1.25×10^{-3}	Segmentation	16	2.9×10^{-1}	4.6

6.2. **Refinement study and CPU-time scaling.** To investigate the behaviour under refinement, we performed a sequence of experiments for the Burgers travelling-wave with fixed viscosity and final time, varying the Haar resolution level J, the number of segments N_{seg} in the segmentation method and the time step Δt. For each configuration we recorded the L^∞ error and the CPU time (in arbitrary units). A representative subset of the results is reported in Table 2.

The values in Table 2 illustrate three trends.

- For all schemes the error decreases as J increases and Δt is halved, but the segmentation method consistently yields the smallest L^∞ error at each resolution level.
- The CPU time for segmentation is comparable to, and sometimes slightly lower than, that of RK4 and Bernoulli at the same resolution, despite the overhead of handling multiple segments.
- The error reduction factor for segmentation as J increases from 2 to 4 is approximately an order of magnitude, reflecting the joint effect of higher spatial resolution and better conditioning of the local Haar matrices.

We also checked the sensitivity of the segmentation method by varying one parameter at a time around the baseline Burgers-wave computation. The results are reported in Table 3. They show that the error is most sensitive to the Haar resolution and the number of segments, while the time step mainly affects the result once it approaches the stability limit.

TABLE 3. Sensitivity of the segmentation method for the Burgers travelling wave.

J	N_{seg}	Δt	L_∞	Observation
3	4	2.5×10^{-3}	9.6×10^{-1}	fewer segments
3	8	2.5×10^{-3}	6.8×10^{-1}	baseline
3	12	2.5×10^{-3}	5.9×10^{-1}	improved interface resolution
3	8	5.0×10^{-3}	8.1×10^{-1}	larger time step
3	8	1.25×10^{-3}	6.2×10^{-1}	smaller time step
4	8	2.5×10^{-3}	4.1×10^{-1}	higher Haar resolution

To emphasise the cost/accuracy trade-off, Table 4 summarises the qualitative properties of the three schemes.

TABLE 4. Qualitative comparison of the three schemes.

Property	RK4	Bernoulli	Segmentation
Time accuracy order	4	2	4 (local)
Stability on fine grids	moderate	good	very good
Conditioning of matrices	n/a (explicit)	moderate	best (local blocks)
Handling steep gradients	weakest	medium	strongest
Parallelisation potential	basic	basic	best (per segment)
Overall rating	baseline	compromise	preferred

Tables 2 and 4 together show that segmentation not only matches RK4 and Bernoulli in accuracy for suitable parameters (Table 1) but also achieves markedly smaller errors under systematic refinement at comparable CPU cost. This supports the conclusion that the Haar-based segmentation method is the best overall choice among the three schemes studied here.

7. Conclusion

A unified Haar wavelet segmentation framework has been developed for three classical nonlinear PDEs: the KdV, Sine–Gordon and viscous Burgers equations. Coupled with RK4 time integration, the segmentation method accurately resolves solitary waves, kinks and viscous shocks with relatively few degrees of freedom and exhibits favourable conditioning compared with global Haar collocation. A Bernoulli polynomial collocation scheme offers a compromise between simplicity and accuracy, while a purely global RK4 method of lines is easiest to implement but less robust for strongly nonlinear or sharply varying solutions. Systematic refinement studies demonstrate that, for fixed computational cost, the segmentation approach produces the smallest L^∞ errors and the best stability properties. These features make it a promising candidate for more complex nonlinear wave and shock problems and suggest several directions for future work, including adaptive segment selection and extension to higher-dimensional PDEs.

Acknowledgments

The authors express their sincere gratitude to the anonymous referee for valuable comments and suggestions which helped improve the quality and clarity of the manuscript. The authors also thank the Department of Mathematics and the Department of Physics, Kirori Mal College, University of Delhi, for providing academic support and research facilities.

References

[1] C. Cattani, Haar wavelet splines, *Journal of Interdisciplinary Mathematics*, 4 (2001), 35–47.
[2] C. Cattani, Haar wavelets based technique in evolution problems, *Proceedings of the Estonian Academy of Sciences. Physics and Mathematics*, 53 (2004), 45–63.

[3] C. Cattani and L. M. Sanchez Ruiz, Discrete differential operators in multidimensional Haar wavelet spaces, *International Journal of Mathematics and Mathematical Sciences*, 2004 (41–44) (2004), 2347–2355.
[4] C. Cattani, Harmonic wavelets towards the solution of nonlinear PDE, *Computers & Mathematics with Applications*, 50 (2005), 1191–1210.
[5] C. F. Chen and C. H. Hsiao, Haar wavelet method for solving lumped and distributed-parameter systems, *IEE Proceedings–Control Theory and Applications*, 144 (1997), 87–94.
[6] C. F. Chen and C. H. Hsiao, A Walsh series direct method for solving variational problems, *Journal of the Franklin Institute*, 300 (1975), 265–280.
[7] M. Devi, S. Sharma and S. Rawan, Numerical solutions of system of linear differential equations using Haar wavelet approach, *Poincare Journal of Analysis and Applications*, 10 (2023), no. 1, 61–73. DOI: 10.46753/pjaa.2023.v010i01.005.
[8] B. Hussain, Afroz, and S. Jahan, Approximate solution for proportional-delay Riccati differential equations by Haar wavelet method, *Poincaré Journal of Analysis and Applications*, 8 (2021), no. 2. DOI: 10.46753/pjaa.2021.v08i02.004.
[9] U. Lepik, Numerical solution of differential equations using Haar wavelets, *Mathematics and Computers in Simulation*, 68 (2005), 127–143.
[10] H. Rezazadeh and M. Shahmorad, A collocation method based on Bernoulli polynomials for nonlinear boundary value problems, *Applied Mathematics and Computation*, 274 (2016), 274–285.
[11] J. K. Sahani, P. Kumar, A. Kumar and N. Khanna, Numerical solution of non-linear Liénard equation using Haar wavelet method, *Poincare Journal of Analysis and Applications*, 11 (2024), no. 2, 197–210. DOI: 10.46753/pjaa.2024.v011i02.009.
[12] I. Singh and M. Kaur, Wavelet methods for solving third-order ordinary differential equations, *International Journal of Applied Mathematics*, 34 (2021), 1171–1186.
[13] R. S. Stanković and B. J. Falkowski, The Haar wavelet transform: its status and achievements, *Computers & Electrical Engineering*, 29 (2003), 25–44.
[14] G. Strang and T. Nguyen, *Wavelets and Filter Banks*, Wellesley–Cambridge Press, 1997.
[15] Y. You and S. Fang, Bernoulli polynomial solutions for differential equations, *Applied Mathematics and Computation*, 95 (1998), 241–254.